Journal of Radiation Research, 2015, 56, 197–204
doi: 10.1093/jrr/rru076 Advance Access Publication 10 September 2014

Radial dependence of lineal energy distribution of 290-MeV/u carbon and 500-MeV/u iron ion beams using a wall-less tissue-equivalent proportional counter

Shuichi TSUDA[1,*], Tatsuhiko SATO[1], Ritsuko WATANABE[2] and Masashi TAKADA[3]

[1]Research Group for Radiation Protection, Japan Atomic Energy Agency, 2-4, Shirakata-shirane, Tokai-mura, Naka-gun, Ibaraki 319-1195, Japan
[2]Research Group for Radiation Effect Analysis, Japan Atomic Energy Agency, 2-4, Shirakata-shirane, Tokai-mura, Naka-gun, Ibaraki 319-1195, Japan
[3]Department of Technical Support and Development Fundamental Technology Center, National Institute of Radiological Sciences, 4-9-1, Anagawa, Inage-ku, Chiba 263-8555, Japan
*Corresponding author. Research Group for Radiation Protection, Japan Atomic Energy Agency, 2-4, Shirakata-shirane, Tokai-mura, Naka-gun, Ibaraki 319-1195, Japan. Tel: +81-29-282-5242; Fax: +81-29-282-6768; Email: tsuda.shuichi@jaea.go.jp

(Received 28 February 2014; revised 15 July 2014; accepted 11 August 2014)

Using a wall-less tissue-equivalent proportional counter for a 0.72-μm site in tissue, we measured the radial dependence of the lineal energy distribution, $yf(y)$, of 290-MeV/u carbon ions and 500-MeV/u iron ion beams. The measured $yf(y)$ distributions and the dose-mean of y, $\bar{y}_D$, were compared with calculations performed with the track structure simulation code TRACION and the microdosimetric function of the Particle and Heavy Ion Transport code System (PHITS). The values of the measured $\bar{y}_D$ were consistent with calculated results within an error of 2%, but differences in the shape of $yf(y)$ were observed for iron ion irradiation. This result indicates that further improvement of the calculation model for $yf(y)$ distribution in PHITS is needed for the analytical function that describes energy deposition by delta rays, particularly for primary ions having linear energy transfer in excess of a few hundred keV μm^{-1}.

Keywords: heavy ion; lineal energy; wall-less tissue-equivalent proportional counter; radial dependence

INTRODUCTION

Cancer therapy by energetic ion beams has been a well-established clinical technique since the 1990s [1, 2]. Energetic ion beams interact with nuclei in the human body and create various secondary particles that can deposit energies in tumors or normal tissue. To estimate the radiological effect of charged particles on the human body with the requisite precision necessary to perform treatment planning, computer simulation has become a powerful and indispensable tool.

Simulations that model cell survival following exposure to charged particles have been developed and incorporated into simulation code systems in order to calculate biological dose for treatment planning [3–5]. Although calculations that use Monte Carlo techniques were impractical in the early 1990s because of scarce computer resources, more sophisticated and practical models have recently been developed [6–9] based on deposited energy distributions of microdosimetric quantities [10], such as lineal energy y or specific energy z.

A microdosimetric kinetic model (MKM) [6] employed for biological dose calculation enables one to obtain relative biological effectiveness (RBE) based on y, which is defined as energy deposition per average chord length in a microscopic region [10]. The lineal energy distribution $yf(y)$ can be obtained by a microdosimetric function [11] incorporated in the Particle and Heavy Ion Transport code System (PHITS) [12, 13]. The microdosimetric function allows the $yf(y)$ distributions originally calculated by a track structure simulation to be instantly reproduced. The microdosimetric functions are expressed by a combination of numerical functions that have been systematically verified against experimental data for broad ion beams of protons, helium, carbon, silicon and iron [14–16]. The calculated values are consistent with the

measured dose-mean lineal energies [15, 16] within an error of 20% for y ranging from ~3 to ~300 keV μm^{-1}. However, in some cases, the shape of the measured $yf(y)$ distribution differs from the calculation, particularly in the range of y that receives contributions from primary ions and secondary electrons (delta rays). This is a problem because the exact shape of the $yf(y)$ distribution is essential for modern biological dose calculation models [9] to estimate precise RBE values. The difference cannot be further investigated based on the data alone, because data acquired from a broad beam provide information on mixed $yf(y)$ distributions with contributions from both primary ions and delta rays.

To further investigate the characteristics of the $yf(y)$ distribution arising from both primary ions and secondary particles, measurements of the $yf(y)$ distribution have been performed using radially scanning narrow energetic heavy ion beams against the beam path. To obtain the $yf(y)$ distribution of primary ions and delta rays separately, 500-MeV/u iron ion beams with high linear energy transfer (LET) were employed in the narrow beam irradiation condition, in addition to 290-MeV/u carbon ion beams commonly used in particle therapy. This paper reports the radially measured $yf(y)$ distributions. Furthermore, we obtained the radially integrated $yf(y)$ distributions and compared them with those calculated by PHITS. Finally, the differences in the $yf(y)$ distributions and dose-mean values of y are also discussed.

MATERIALS AND METHODS

Experiment

The $yf(y)$ distributions were measured for 290-MeV/u carbon ions and 500-MeV/u iron ions at the HIMAC-BIO beam line at the Heavy Ion Medical Accelerator in Chiba (HIMAC) [1], part of the National Institute of Radiological Science (NIRS), Japan. The ion beams from the synchrotron accelerator passing through 10 m of air were collimated by brass blocks into a low divergence beam and guided to a wall-less tissue-equivalent proportional counter (wall-less TEPC) [15, 16] followed by a beam monitor and beam dump. Figures 1 and 2 show the experimental setup at HIMAC-BIO.

From recent dosimetric studies, we know it is essential to use wall-less TEPCs to measure $yf(y)$ distributions for energetic heavy ions because of wall effects [10, 14–18]. The wall-less TEPC used in the present study has a cylindrical detection part (3 mm in both length and diameter) and is in essence the same detector as previously reported [15, 16] except that it had a different container. The container used in the present study has two windows comprising a 50-μm-thick Kapton film for beam entrance and exit. This arrangement allows incident ions to pass through the detector so that the beam position can be monitored without producing superfluous secondary radiations. The container was filled with a propane-based tissue-equivalent gas [10] (TE-gas) at a pressure of 13.3 kPa (100 Torr). At this pressure, the gas is equivalent to a cylindrical site in tissue measuring 0.72 μm in both length and diameter. The applied potentials were −800 V to the cathode, 0 V to the anode (GND), and −665 V to the field tubes. The signals passing through a pre-amplifier were amplified by a linear amplifier and then split into three channels in a digital storage oscilloscope (DSO) to gain a large dynamic range (up to three digits) [15].

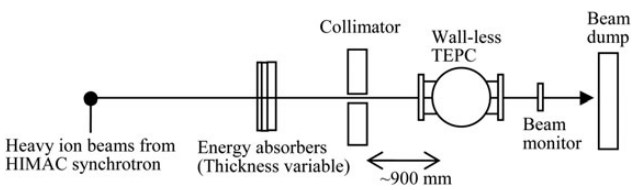

Fig. 1. Experimental setup at HIMAC-BIO (not to scale).

The pulse-height distributions of the ion beams obtained by the DSO were converted into y distributions on the basis of energy calibration against a surface source of ^{244}Cm ($E_\alpha = 5.78$ MeV) installed inside the wall-less TEPC. The distance between the center of the source and the anode was maintained at 7 mm during the calibration, which was conducted before and after each measurement. The details of the experimental conditions are reported elsewhere [15].

The ion beam parameters are shown in Table 1. For 500-MeV/u iron ions, a set of energy absorbers composed of acryl with 51.8-mm water-equivalent thickness was utilized to enhance the LET of the primary beam. The energy loss before the beam enters the wall-less TEPC is also listed in Table 1. The SRIM code [19] was used to estimate energy loss and the LET of the primary ions. The values of the LET are the same as the stopping power (dE/dx) in water. The collimator hole size was 1 mm^2. The beam diameter at the measurement position in the wall-less TEPC, however, was estimated to be 2–3 mm using a photosensitive paper.

To monitor the number of ions incident on the wall-less TEPC, we used 16 scintillation fibers, each with a 1 mm^2 cross section (Saint-Gobain Crystals). A schematic of the beam monitor is shown in Fig. 3. Each detected signal was separately transmitted through 1-m-long scintillation fibers

Table 1. Parameters of ion beam incident on wall-less TEPC

No.	Ions	Incident energy (MeV/u)	Energy loss (MeV/u)		Energy at wall-less TEPC (MeV/u)	LET (keV μm^{-1})
			in air	in absorber		
I	C^{6+}	290	12.3	0.0	278	13.0
II	Fe^{26+}	500	37.7	0.0	462	189
III	Fe^{26+}	500	37.7	197	266	251

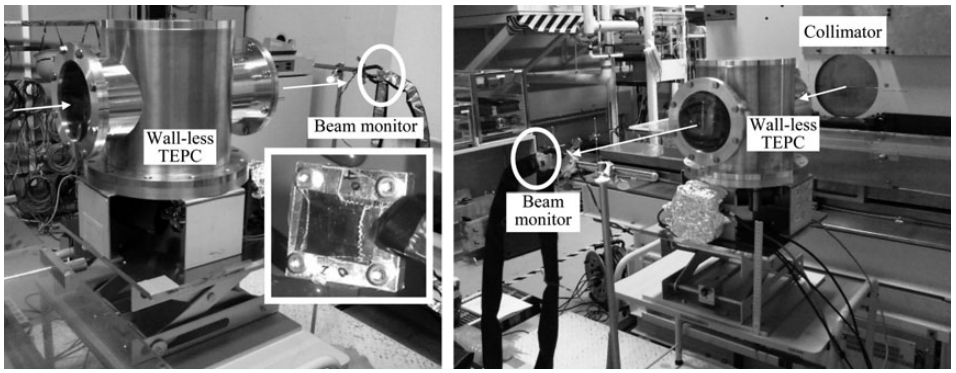

Fig. 2. Photographs of experiment at HIMAC-BIO. The arrows show the ion beam path.

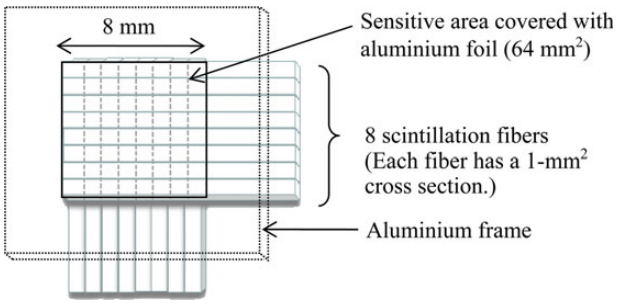

Fig. 3. Schematic of beam monitor comprising 16 scintillation fibers.

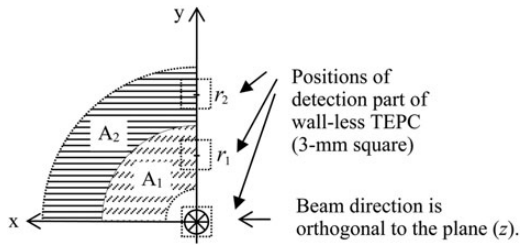

Fig. 4. Arrangement of wall-less TEPC with respect to beam path. The beam direction is orthogonal to the x–y plane at $(x, y) = (0.0, 0.0)$.

to a 16-channel multi-anode photomultiplier (H8711, HAMAMATSU PHOTONICS KK). The sensitive area of the beam monitor was 64 mm^2 and was covered with aluminum foil. By simultaneously counting the signals from laterally and vertically arranged scintillation fibers, 64 positions at intervals of 1 mm were independently monitored during irradiation. The projected area (3 mm^2) of the wall-less TEPC was completely covered by the sensitive area of the beam monitor. Coincidence measurements were performed between the wall-less TEPC and the beam monitor to sample single-ion events with the DSO.

During the measurement, the beam monitor was fixed and aligned to the incident beam direction. Figure 4 shows the arrangement of the wall-less TEPC. By putting the wall-less TEPC on a movable stand, the height of the detection part of the wall-less TEPC could be changed with respect to the beam path to investigate the radial dependence of the $yf(y)$ distributions. For example, the measured $yf(y)$ at a distance r_1 ($= y_1$) is represented by the area A_1 in Fig. 4. The precision of the height adjustment is <1 mm. The uncertainty in the radial distance r from the beam path was estimated to be ±1.5 mm, which is equivalent to ± 0.36 µm in tissue (by taking the beam cross section and the uncertainty of the lateral positions of the beam monitor into account).

Dose-mean lineal energy

The dose-mean lineal energy $\bar{y}_D$ is obtained from the $yf(y)$ distribution as follows [10]:

$$\bar{y}_D = \int_{y_{min}}^{y_{max}} y d(y) dy = \int_{y_{min}}^{y_{max}} y^2 f(y) dy \Big/ \int_{y_{min}}^{y_{max}} y f(y) dy, \qquad (1)$$

where $d(y)$ is the dose probability density of y. y_{max} and y_{min} are the maximum and the minimum values of y, respectively. Because the values of y_{min} are based on noise levels under experimental conditions, the $\bar{y}_D$ obtained experimentally is restricted and differs from what would be obtained under ideal conditions (i.e. for $y_{min} = 0$). Note that $\bar{y}_D$ is less sensitive to a change in y_{min} than is $\bar{y}_F$, which is the frequency-mean of y.

RESULTS AND DISCUSSION

Pulse-height distributions

Data analysis is based on the waveforms from the wall-less TEPC with the beam monitor offline. Figure 5 shows the measured pulse-height distributions of ion beams of 290-MeV/u carbon and 500-MeV/u iron. The uncertainties represent one standard deviation. The counts are normalized

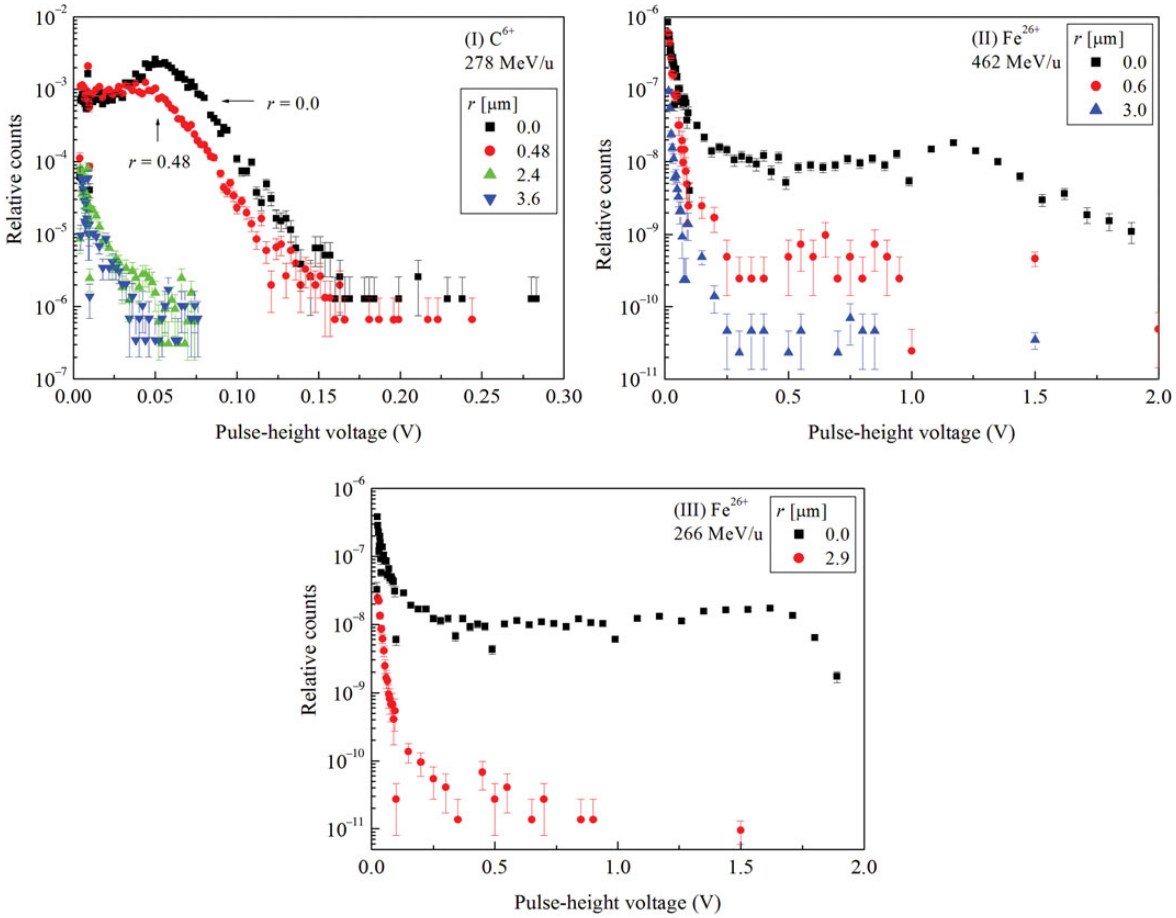

Fig. 5. Pulse-height distributions for (**I**) carbon ions and (**II** and **III**) iron ions measured at the radial distances shown in the legends.

by the number of events that are monitored by both the wall-less TEPC and the beam monitor in coincidence. The radial distance from the beam path shown in the legends is in the microdosimetric scale. In Fig. 5I, the peak of the incident carbon ions is at ~0.05 V, and that of the delta rays is below ~0.02 V. The distribution at $r = 0.48$ μm includes contributions from both the carbon ion beam and delta rays. In the distribution at $r = 2.4$ and 3.6 μm, however, some contributions appear above 0.02 V, which could be due to electrical noise. The distribution at $r = 2.4$ μm is similar to that at $r = 3.6$ μm, which is consistent with the results of Metting *et al.* [14] and Schmollack *et al.* [18] for measurements far from the beam path. For iron ions (Fig. 5II), the peak of the primary iron ions is at ~1.2 V, and the contributions of iron ions and delta rays appear in the distribution for $r = 0.6$ μm. Signals greater than ~0.2 V in the distribution for $r = 3.0$ μm are contaminated by electrical noise. Several counts of up to 0.8 V are also observed in Fig. 5III.

Lineal energy distributions

Figure 6 shows the distributions $yf_r(y)$ converted from the pulse-height distributions measured at various radial distances r. Each distribution is normalized by the number of events on both the wall-less TEPC and the beam monitor in coincidence. In Fig. 6I, the main peak of the 278-MeV/u carbon ion beam appears clearly at $r = 0.0$ μm. The beam passing through the detection part forms a peak that depends on the chord length of the cylindrical detector. A similar broad peak is also found for $r = 0.48$ μm, along with a contribution from delta rays. For $r \geq 2.4$ μm, the results are almost entirely due to delta rays, although the contribution at >10 keV μm^{-1} is partially attributable to electrical noise, as indicated by the data.

For the iron ions (Fig. 6II and 6III), even for $r = 0.0$ μm, the contribution of delta rays appears along with the peaks from the primary ions that have passed through the detector. Since the sizes of the detection part and the collimated beam are comparable in size at the position of the wall-less TEPC, delta rays produced outside the detection part would also be detected.

To compare the results with the other measurements or the calculation, the $yf_r(y)$ distributions were integrated over r. The frequency distribution of y integrated in the radial direction is:

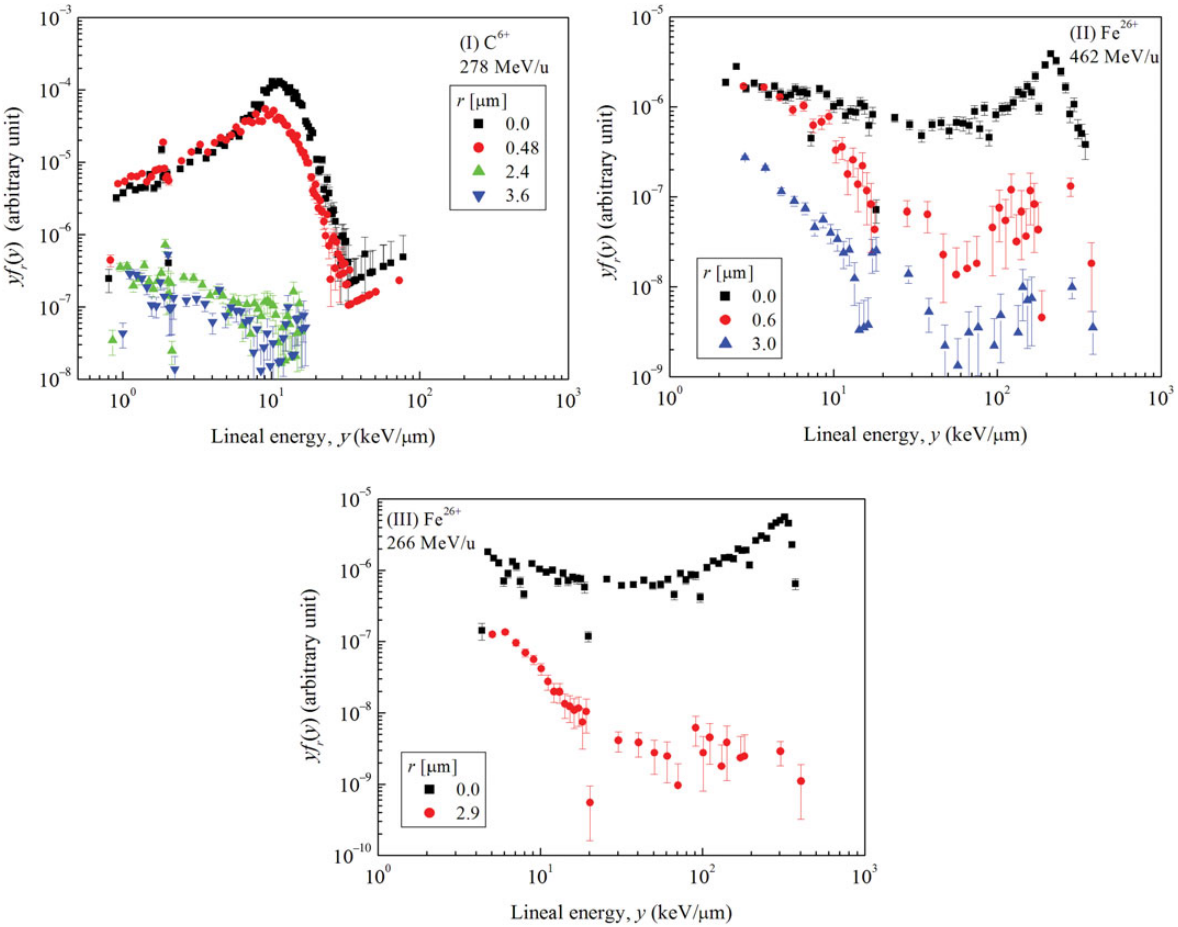

Fig. 6. Lineal energy distributions at radial directions for (**I**) 290-MeV/u carbon ions and (**II** and **III**) 500-MeV/u iron ions.

$$f(y) = \int_0^{r_{max}} rR_r f_r(y)dr \Big/ \int_0^{r_{max}} rR_r dr, \qquad (2)$$

where R_r is the relative probability of a single-event per incident primary ion occurring in the detection part of the wall-less TEPC, r_{max} is the maximum radial distance, and $f_r(y)$ denotes the frequency distribution measured at distance r. The value of R_r is determined by the number of ions detected in both the wall-less TEPC and the beam monitor, and that incident on the beam monitor.

The radially integrated $yf(y)$ distribution obtained from Eq. (2) is shown in Fig. 7, along with the $yf(y)$ distribution for a broad beam of 290-MeV/u carbon ions [15]. The size of the simulated site of the reference was the same as that employed in the present study. The radius of the broad beam was ~50 mm, which is equivalent to 12 μm in the microdosimetric scale. The lower limit of y in this study was higher than that for the broad beam irradiation because of the difference in experimental conditions. The areas under the curves were normalized to unity, and the uncertainties are negligibly small. The integrated $yf(y)$ was fairly consistent with $yf(y)$ obtained with broad beam irradiation.

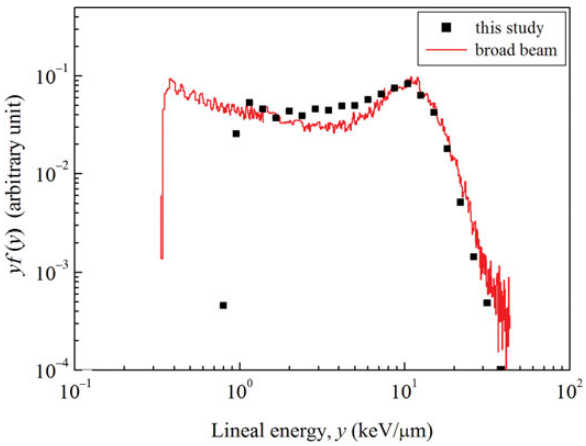

Fig. 7. Radially integrated $yf(y)$ distribution obtained with a pencil beam (this study) compared with that obtained with a broad beam (12 μm radius) of 290-MeV/u carbon ions [15].

Comparison with Monte Carlo simulation

Figures 8 and 9 present the $yf_r(y)$ distributions measured in the radial direction for 290-MeV/u carbon ions and for 500-MeV/u iron ions, respectively, along with calculated results. The areas under the data curves are normalized to unity. The calculations were performed using the Monte Carlo track structure simulation code TRACION [20], which explicitly treats all physical processes such as ionization and excitation of electrons in calculating the track structure in water on a nanometer scale. The $yf_r(y)$ distributions are obtained based on the results calculated by TRACION.

The measurements are fairly consistent with the calculation shown in Fig. 8, although the range of the measured distributions is limited and the uncertainties in the results at $r = 3.6$ μm are relatively large for both calculation and measurement because of rare delta ray events. For iron ions at $r = 0.0$ μm (Fig. 9), the measured distribution ranges from ~2 to ~200 keV μm^{-1}, whereas the calculated distribution ranges from ~30 to ~200 keV μm^{-1}. This difference could be attributable to delta rays produced near the detection part of the wall-less TEPC, as already mentioned.

Figure 10 compares radially integrated $yf(y)$ distributions with calculations by the microdosimetric function [11] of PHITS. The spectra of $yf(y)$ calculated by PHITS have become wider because of the energy resolution in the full width at half maximum (FWHM) in the measurement. The statistical uncertainty for the PHITS calculation is too small to be observed in Fig. 10. The dose-mean lineal energies calculated by Eq. (1) are shown in Table 2. The uncertainty in $\bar{y}_D$ is estimated to be 10% [15]. In Fig. 10I, the peak position and the region with delta rays (approximately a few keV/μm) are fairly consistent with the calculation.

In Fig. 10II and III and for $y > 10$ keV μm^{-1}, large fluctuations in the experimental data result from the small number of counts measured at distances away from the beam path, as shown in Fig. 5. The values of $\bar{y}_D$ obtained from the measurement and those obtained from the calculation in Table 2 agree within an error of 2%. This result is consistent with

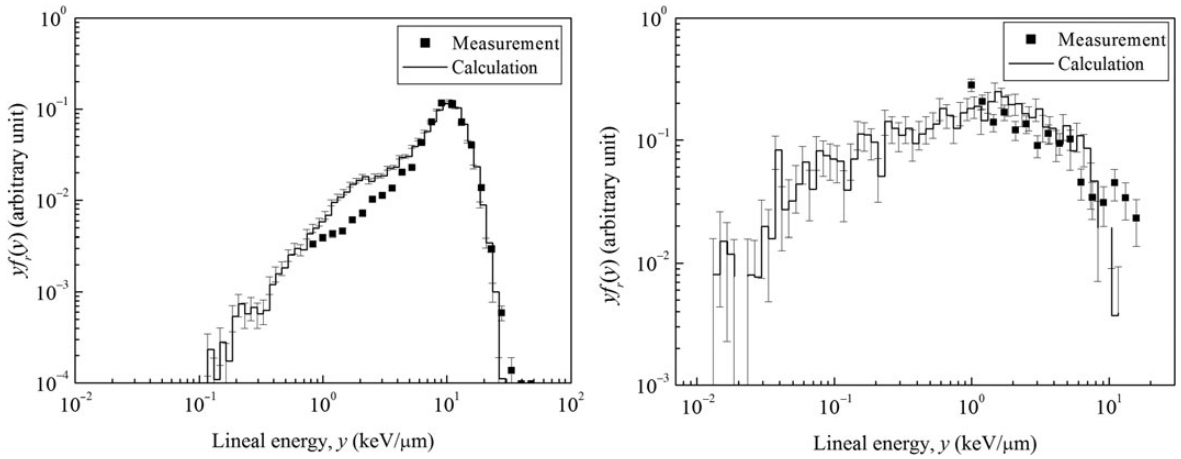

Fig. 8. $yf_r(y)$ distributions for 290-MeV/u primary carbon ions at (left) $r = 0.0$ μm and (right) $r = 3.6$ μm.

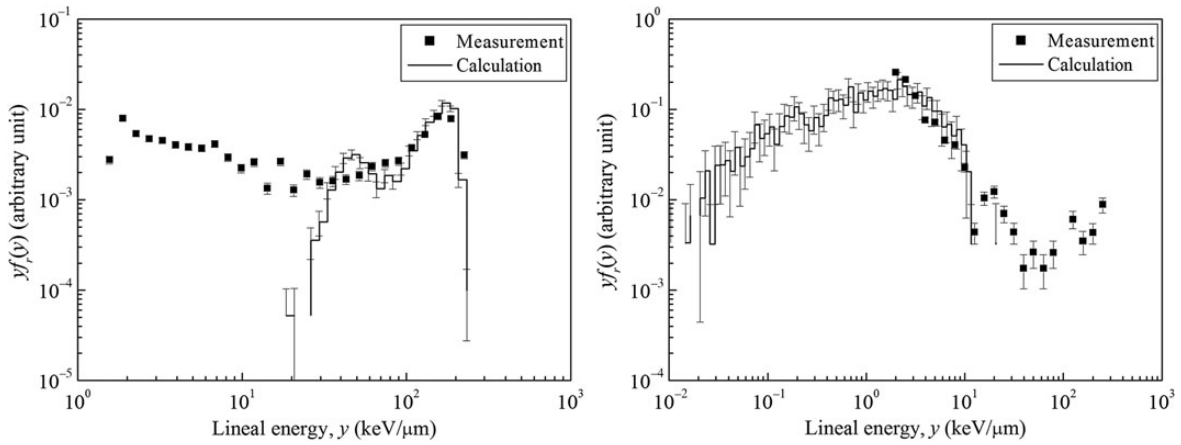

Fig. 9. $yf_r(y)$ distributions for 500-MeV/u primary iron ions at (left) $r = 0.0$ μm and (right) $r = 3.0$ μm.

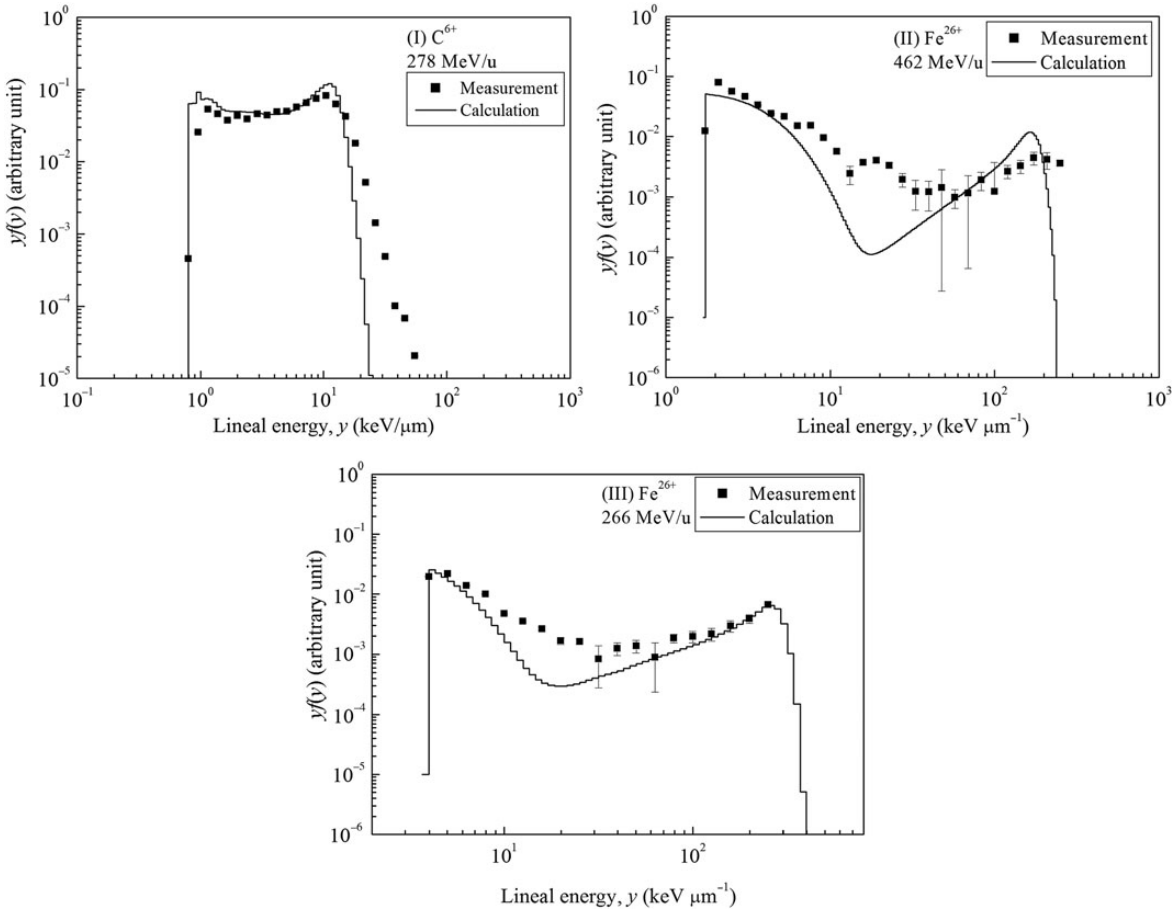

Fig. 10. Radially integrated lineal energy distributions for 500 MeV/u iron ions in radial directions, along with distribution calculated by PHITS.

Table 2. Measured dose-mean lineal energies compared with those obtained by PHITS calculation

		Incident energy	$\bar{y}_D$ (keV μm^{-1})		
No.	**Ions**	**(MeV/u)**	**Experiment**	**Calculation**	**Calc./Exp.**
II	Fe^{26+}	462	131 ± 13	128 ± 0.1	0.98 ± 0.1
III	Fe^{26+}	266	170 ± 17	172 ± 0.1	1.01 ± 0.1

previous data [16] acquired using a broad heavy ion beam with a LET of up to ~300 keV μm^{-1}. However, the measured spectra are an order of magnitude larger than the calculated spectra for y ranging from 10–30 keV μm^{-1}, which is the valley between the peaks of iron ions and the plateau of delta rays. The large valley in the PHITS calculation is attributed to the model of the microdosimetric function [11], which reproduces $yf(y)$ distributions obtained by a track structure calculation [20]. In PHITS, the analytical functions consist of two independent distributions for primary ions and delta rays. The probability density for primary ions is based on chord lengths. Although the valley is formed by a combination of the two distributions, the valley between primary ions and delta rays could appear substantially greater for incident ions with a LET in excess of a few hundred keV μm^{-1}. If the LET of primary ions is several tens of keV μm^{-1}, as for the 290-MeV/u carbon ions used in this study, the valley is not so apparent because the functions overlap.

The result in Fig. 10III differs from the result in Fig. 10II because some secondary particles produced through nuclear reactions [21, 22] enter the wall-less TEPC and contribute to the $yf(y)$ distribution. This result is attributed to the energy

absorbers that were used in condition (III) to decrease the energy of the iron ions. The difference between experiment and calculation is similar to that for Fig. 10II, although energetic fragments such as protons and helium contribute to y from ~10 to ~100 keV μm^{-1}.

In conclusion, using a wall-less TEPC equivalent for a 0.72 μm tissue site, we experimentally evaluated the radial dependence of $yf(y)$ for ion beams of 290-MeV/u carbon ions and 500-MeV/u iron ions. The values of $\bar{y}_D$ calculated by PHITS were consistent with the measured values of $\bar{y}_D$ within an error of 2%, even when energetic secondary particles were produced through nuclear reactions by high-energy iron ions (500 MeV/u) with a high atomic number ($Z = 26$). However, the $yf(y)$ distributions calculated by PHITS for 500-MeV/u iron ions were smaller than the measured distributions for y, ranging from 8–30 keV μm^{-1}. Thus, the microdosimetric function used by PHITS must be improved to more precisely estimate $yf(y)$ distributions, particularly for primary ions having a LET in excess of a few hundred keV μm^{-1}. A recent study [9] reported that the shape of $yf(y)$, as well as the mean value of $yf(y)$, $\bar{y}_D$, is necessary to better estimate the RBE. Thus, the data obtained in this study could be useful for clinical applications, because the RBE-weighted dose is an important index used in particle therapy.

ACKNOWLEDGEMENTS

The authors thank Dr T. Murakami and the technical staff of HIMAC for providing their generous support during the experiments. The present work was performed under the Research Project with Heavy Ions at NIRS-HIMAC: 23P237.

FUNDING

Funding to pay the Open Access publication charges for this article was provided by Japan Atomic Energy Agency.

REFERENCES

1. Hirao Y, Ogawa H, Yamada S *et al*. Heavy-ion synchrotron for medical use – HIMAC project at NIRS JAPAN. *Nucl Phys A* 1992;**538**:541c–50c.
2. Kraft G, Arndt U, Becher W *et al*. Heavy ion therapy at GSI. *Nucl Instrum Methods Phys Res A* 1995;**367**:66–70.
3. Kanai T, Furusawa Y, Fukutsu K *et al*. Irradiation of mixed beam and design of spread-out Bragg peak for heavy-ion radiotherapy. *Radiat Res* 1997;**147**:78–85.
4. Scholz M, Kraft G. Calculation of heavy ion inactivation probabilities based on track structure, X-ray sensitivity and target size. *Radiat Prot Dosimetry* 1994;**52**:29–33.
5. Krämer M, Jäkel O, Haberer T *et al*. Treatment planning for heavy-ion radiotherapy: physical beam model and dose optimization. *Phys Med Biol* 2000;**45**:3299–317.
6. Kase Y, Kanai T, Matsumoto Y *et al*. Microdosimetric measurements and estimation of human cell survival for heavy-ion beams. *Radiat Res* 2006;**166**:629–38.
7. Inaniwa T, Furukawa T, Kase Y *et al*. Treatment planning for a scanned carbon bean with a modified microdosimetric kinetic model. *Phys Med Biol* 2010;**55**:6721–37.
8. Sato T, Kase Y, Watanabe R *et al*. Biological dose estimation for charged-particle therapy using an improved PHITS code coupled with a microdosimetric kinetic model. *Radiat Res* 2009;**171**:107–17.
9. Sato T, Furusawa Y. Cell survival fraction estimation based on the probability densities of domain and cell nucleus specific energies using improved microdosimetric kinetic models. *Radiat Res* 2012;**178**:341–56.
10. ICRU (International Commission on Radiation Units and Measurements). Microdosimetry. *ICRU Report 36*. Bethesda, MD, 1983.
11. Sato T, Watanabe R, Niita K. Development of a calculation method for estimating specific energy distribution in complex radiation fields. *Radiat Prot Dosimetry* 2006;**122**:41–5.
12. Niita K, Matsuda N, Iwamoto H *et al*. PHITS: Particle and Heavy Ion Transport code System, version 2.23, JAEA-Data/Code 2010-022, 2010.
13. Iwase H, Niita K, Nakamura T. Development of a general-purpose particle and heavy ion transport Monte Carlo code. *J Nucl Sci Technol* 2002;**39**:1142–51.
14. Metting NF, Rossi HH, Braby LA *et al*. Microdosimetry near the trajectory of high-energy heavy ions. *Radiat Res* 1988; **116**:183–95.
15. Tsuda S, Sato T, Takahashi F *et al*. Measurement of microdosimetric spectra with a wall-less tissue-equivalent proportional counter for a 290 MeV/u ^{12}C beam. *Phys Med Biol* 2010; **55**:5089–101.
16. Tsuda S, Sato T, Takahashi F *et al*. Systematic measurement of lineal energy distributions for proton, He and Si ion beams over a wide energy range using a wall-less tissue equivalent proportional counter. *J Radiat Res* 2012;**53**:264–71.
17. Tsuda S, Sato T, Takahashi F *et al*. Analysis of the effect of structural materials in a wall-less tissue equivalent proportional counter irradiated by 290 MeV/u carbon beam. *Radiat Prot Dosimetry* 2011;**143**:450–4.
18. Schmollack JU, Klaumuenzer SL, Kiefer J. Stochastic radial dose distributions and track structure theory. *Radiat Res* 2000; **153**;469–78.
19. Ziegler JF, Biesak JP, Littmark U. *The stopping and range of ions in solids. The stopping and range of ions in matter*, *Vol. 1*. Ziegler JF (ed.), New York: Pergamon, 1985.
20. Watanabe R, Wada S, Funayama T *et al*. Monte Carlo simulation of radial distribution of DNA strand breaks along the C and Ne ion paths. *Radiat Prot Dosimetry* 2011;**143**:186–90.
21. Matsufuji N, Komori M, Sasaki H *et al*. Spatial fragment distribution from a therapeutic pencil-like carbon beam in water. *Phys Med Biol* 2010;**50**:3393–403.
22. Haettner E, Iwase H, Schardt D. Experimental fragmentation studies with ^{12}C therapy beams. *Radiat Prot Dosimetry* 2006; **122**:485–7.